

Low Multipoles Anomalies of CMB Maps

O.V. Verkhodanov¹

E-mail: *vo@sao.ru*

We consider anomalies of cosmic microwave background observed at low multipoles of the WMAP and Planck cosmic missions. The possible origin of these features is discussed. We study difference of both missions data which is apparently connected with the local sources emission and/or systematics.

1 Introduction

The last decade of the cosmic microwave background (CMB) study was marked by several marvelous discoveries which changed the observational cosmology. The main cosmological parameters were measured with two satellites – WMAP and Planck.

The observations of the CMB radiation by the Wilkinson Microwave Anisotropy Probe (WMAP, <http://lambda.gsfc.nasa.gov>) [1, 2] were revolutionary in modern cosmology. The data were recorded in five bands: 23, 33, 41, 61, and 94 GHz with the measurements of intensity and polarization. The mission results include the CMB maps of anisotropy and polarization, the maps of foreground components (synchrotron and free-free emission, dust radiation), their power spectrum. The resolution of the CMB map restored with implementing the Internal Linear Combination (ILC) method [1] is 40'. The angular power spectrum of CMB produced by the WMAP experiment allowed one to measure all the main cosmological parameters at the most precise level of observational cosmology (with accuracy less than 10%) [3].

The second set of maps and corresponding data were obtained in the European Space Agency experiment Planck (<http://www.rssd.esa.int/Planck/>) [4] and produced new possibilities in investigation of foreground components and radio sources in millimeter and submillimeter wavelengths. Planck observations were carried out at low frequency instrument (LFI bandwidths: 30, 44, 70 GHz) and high frequency instrument (HFI bandwidths: 100, 143, 217, 353, 545, 857 GHz). The resolution of the Planck CMB maps is $\sim 5'$. The Planck mission allowed one to obtain new and independent observational data.

Results of both experiments also contain some anomalies violated our expectation from the CMB Gaussian distribution. The most discussed ones [5] are Axis of Evil [6], Cold Spot [7], violation of parity in the power spectrum [8], asymmetry “North – South” in galactic coordinate system [9]. The Planck data

¹ Special astrophysical observatory RAS, Nizhnij Arkhyz, Russia

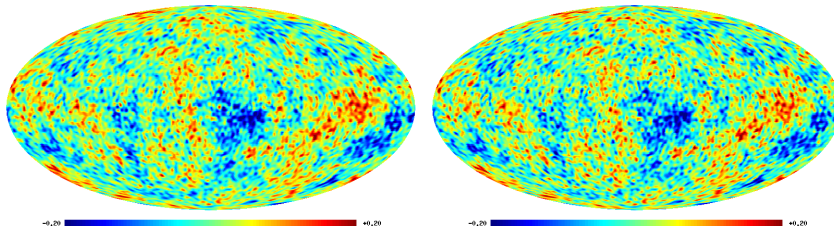


Figure 1: CMB maps restored from the WMAP (left, ILC map) and Planck (right, SMICA map) observational data and smoothed upto $\ell_{\max} = 100$.

added a new unexpected phenomena – too low amplitude of low harmonics [10]. All these anomalies occur at the largest angular scales ($\theta > 1^\circ$) and demonstrate observation statistical anisotropy being a sign of non-Gaussianity at low multipoles.

There are two basic approaches in understanding the origin of anomalies. The first one is based on suggestion of complex processes during early stages of the Universe. The second one follows the idea of connection of the anomalies with foregrounds and/or data analysis procedures.

Two basic properties of CMB allow one to separate its signal from foregrounds: (1) black body emission, so it has the same temperature at all wavelengths, and (2) correlation of CMB and foregrounds should be close to zero, because CMB is a random Gaussian process. In the simple case, the sought ILC temperature can be written as a linear combination of signal from the maps for different frequencies. The different versions of the ILC method and its variations exist both in pixel space and in harmonic space [11]. The maps restored in WMAP and Planck experiments are shown in Fig. 1.

For the restored CMB signal, the angular power spectrum is calculated using the so called $a_{\ell m}$ -coefficients $C(\ell) = \frac{1}{2\ell+1} \sum_{m=-\ell}^{\ell} |a_{\ell m}|^2$. The $a_{\ell m}$ -coefficients are obtained in the standard decomposition of the measured temperature variations on the sky, $\Delta T(\theta, \phi)$, in spherical harmonics (multipoles):

$$\Delta T(\theta, \phi) = \sum_{\ell=2}^{\infty} \sum_{m=-\ell}^{m=\ell} a_{\ell m} Y_{\ell m}(\theta, \phi). \quad (1)$$

2 The main WMAP and Planck CMB data anomalies

Axis of Evil. The Axis of Evil (Fig. 2) is the most famous among non-Gaussian features of the WMAP CMB data. The Axis unifies some problems which require special explanations. They are the planarity and alignment of the two harmonics, quadrupole and octupole, and, partly, the problem of extremely low amplitude of the quadrupole. Different estimations of the significance of existence of this axis, and several hypotheses on its origin were made. Various studies (e.g., [12, 13]) investigated the contribution of background components and their influence on the alignment of multipoles ($\ell = 2$ and $\ell = 3$), and indicated a small probability

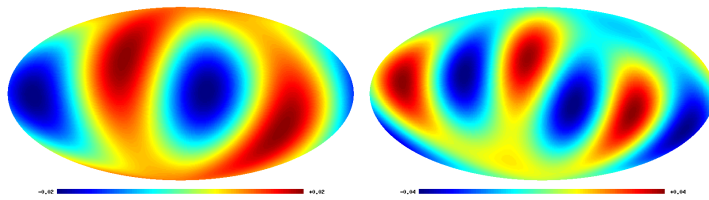


Figure 2: Axis of Evil: planarity and alignment of the quadrupole (left) and the octupole (right) on the WMAP CMB map.

of the background effect on the orientation of the low multipoles. Randomness of such an effect is estimated by the authors as unlikely at the significance level exceeding 98% and excludes the effect of residual contribution of background components.

Some cosmological models were developed to explain the prominence of the axis in the orientation of multipoles. They include the anisotropic expansion of the Universe, rotation and magnetic field [14, 15].

There are some hints demonstrating that the problem of existence of Axis of Evil can be connected with the instability of CMB reconstruction at low multipoles ($2 \leq \ell \leq 10$) in ILC method [16, 17]. Another possible solution of the problem is to construct the separation methods on the homogeneous samples of pixels where possible to tune selection of subsample in such a way that the quadrupole amplitude of the restored map grows and phase changes, so, no axis of evil exists [18].

Using new data, the Planck team [10] detected the angle between planes of quadrupole and octupole is equal $\sim 13^\circ$ (against $\sim 3^\circ$ or $\sim 9^\circ$ for WMAP data at different observational years) and declared that significance of the quadrupole-octupole alignment is substantially smaller than for the WMAP data, falling to almost 98% confidence level. Later, Copi et al. [19] demonstrated that the WMAP and Planck data confirm the alignments of the largest observable CMB modes in the Universe. Using different statistical methods to control the mutual alignment between the quadrupole and octupole, and the alignment of the plane defined by the two harmonics with the dipole direction, the authors obtained that both phenomena are at the greater than 3σ level for Planck CMB maps studied.

Cold Spot. The next exited feature discussed is the Cold Spot (CS) (Fig. 3). This is a cold region exhibiting a complex structure identified in the CMB using spherical Mexican hat wavelets [7]. The non-Gaussianity of the signal in the Southern hemisphere was explained precisely by the existence of this region. The galactic coordinates of center of the spot are $b = -57^\circ, l = 209^\circ$. The probability of the signal in CS, being consistent with the Gaussian model if spherical wavelets are used, is about 0.2% [7]. After obtaining indication of the signal non-Gaussianity at the CS as well as messages on the reduced density of source [20] in smoothed maps of radio survey NVSS at 1.4 GHz, several hypotheses concerning the origin of the Cols Spot were discussed which were related to the integrated Sachs–Wolfe effect, the topological defect, anisotropic expansion, the artifact of data analysis,

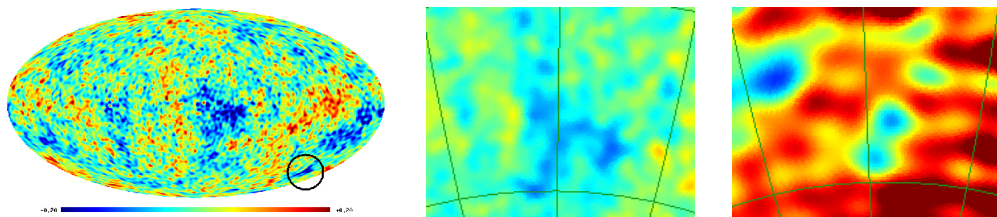


Figure 3: Cold Spot: position of the Cold Spot on the WMAP CMB map (left) and its shape (center) and 408 MHz map (right) with synchrotron emission.

and simply a random deviation (see the review [21]). As was noted in [22], the possible galactic foreground residuals in the CMB maps can produce such a type of the spot as a part of non-Gaussianity at low multipoles. We should add that the CS is also manifested in the data of 1982 in maps of a low-frequency survey where synchrotron radiation contributes significantly to the background (Fig. 3, right). In favor of the hypothesis of the CS being the Galactic phenomena, the following fact testifies. There exists the high correlation of positions of peaks of CMB fluctuation and galactic magnetic field distribution [23].

Violation of the power spectrum parity. A remarkable manifestation of non-Gaussian properties of low multipoles consists in parity asymmetry first noticed in [8] and confirmed in Planck data [10]. For a Gaussian random field of primary perturbations $\Phi(\mathbf{k})$ with a flat power spectrum, the presence of a plateau in the CMB angular power spectrum is expected at low multipoles, which is due to the Sachs–Wolfe effect, namely, to the fact that $\ell(\ell + 1)C_\ell \approx \text{const}$. Spherical harmonics change as $Y_{\ell m}(\hat{\mathbf{n}}) = (-1)^\ell Y_{\ell m}(-\hat{\mathbf{n}})$, when the coordinates are reversed. Therefore, an asymmetry in the angular power spectrum for even and odd harmonics can be regarded as the asymmetry of the power of even and odd components of map. The authors [8] found the power of odd multipoles to systematically exceed the power of even multipoles of low ℓ and termed this phenomenon “parity asymmetry”. To describe such an asymmetry quantitatively, the following quantities are proposed for consideration: $P^+ = \sum_{\text{even } \ell < \ell_{\max}} \ell(\ell + 1)C_\ell/2\pi$, $P^- = \sum_{\text{odd } \ell < \ell_{\max}} \ell(\ell + 1)C_\ell/2\pi$. Using the data of WMAP power spectrum and the results of Monte Carlo simulations, the authors [8] calculated the ratio P^+/P^- for the multipole ranges $2 \leq \ell \leq \ell_{\max}$, where ℓ_{\max} lies between 3 and 23. Comparing P^+/P^- for the WMAP data with the simulated maps ratio allows estimating the quantity p equal to the fraction of simulated spectra in which P^+/P^- is less than or equal to the same quantity for the WMAP map. The value of p was found to reach its lower boundary at $\ell_{\max} = 18$, where p equals 0.004 and 0.001 for the data obtained by the WMAP mission during five and three years of observations, respectively. This fact means that there is a preference for odd multipoles $2 \leq \ell \leq 18$ in the WMAP data at a confidence level of 99.6% with a screening mask imposed on the data, and of 99.76% without any mask. The authors believe the low amplitude of the WMAP CMB quadrupole may be part of the same anomaly as the parity asymmetry.

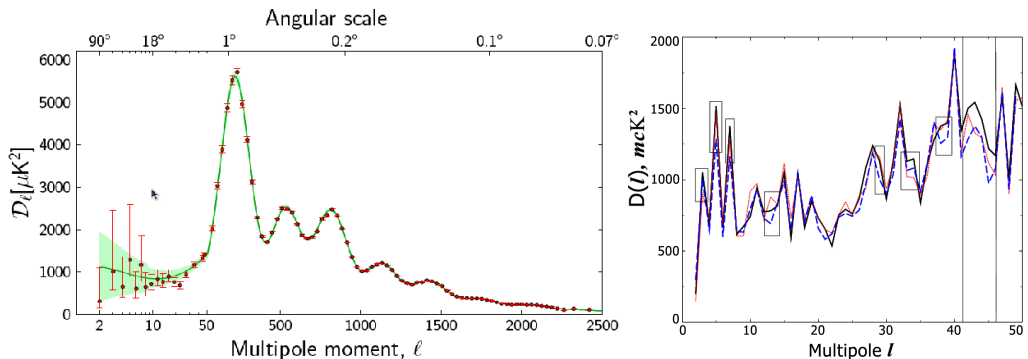


Figure 4: Right: CMB angular power spectrum of the 1st Planck data release. Left: the angular power spectrum $D(\ell) = \ell(\ell + 1)C_\ell/2\pi$ for $2 \leq \ell < 50$. The solid line shows the 7th year WMAP ILC data release. The dotted line marks WMAP9 ILC data. The Planck data are marked by the dashed line. The rectangles show the most different amplitudes. The vertical lines mark limits of $\ell \in [41, 46]$.

Hemispherical Asymmetry. The asymmetry of hemispheres power (see, e.g., Fig. 1) was detected just after publishing the first year all sky maps of the WMAP [9]. Then, in [24], the some calculations based on the angular power spectrum were presented and shown that this spectrum, when estimated locally at different positions on the sphere, appears not to be isotropic. Park [25] also presented evidence for the existence of such hemispherical asymmetry, in which a particular statistical measure is considered to change discontinuously between two hemispheres on the sky, applying Minkowski functionals to the WMAP data. Since the preferred direction according to Eriksen et al. [9] lays close to the ecliptic plane, it was also demonstrated that the large-angular scale N -point correlation functions were different in behavior when computed on ecliptic hemispheres.

The observed properties of the Planck data are consistent with a remarkable lack of power in a direction towards the north ecliptic pole, consistent with the simpler one-point statistics [10].

3 Difference of WMAP and Planck power spectra

One of the main anomalies first detected in the Planck data was the lack of power at low multipoles detected for angular power spectrum $C(\ell)$. Using the WMAP and Planck officially published spectra, we can compare them via the calculation of the difference of maps including only the harmonics with maximum $C(\ell)$ difference (Fig. 4, right).

Following [26], let us consider the differences of maps corresponding to the harmonics having the maximum difference of power. These ranges are marked by rectangles on Fig. 4. The vertical lines demonstrate limits of the multipole range in $\ell \in [41, 46]$. On Figs. 5, 6, there are shown maps of harmonic differences at $\ell = 5$ and $\ell = 7$, respectively. Some features of these differences show the

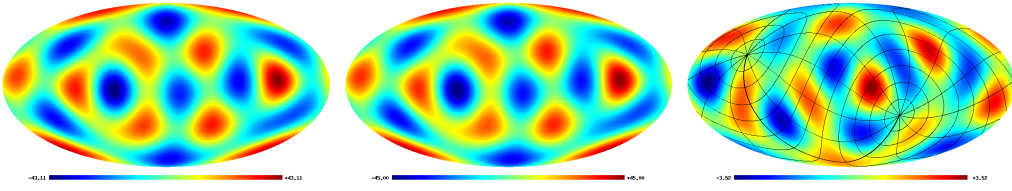


Figure 5: Left to right: the map of $\ell = 5$ of the Planck CMB map SMICA, the $\ell = 5$ of the ILC WMAP9 map, and the map of these signals difference. The equatorial coordinate grid is overlaid on the map of difference.

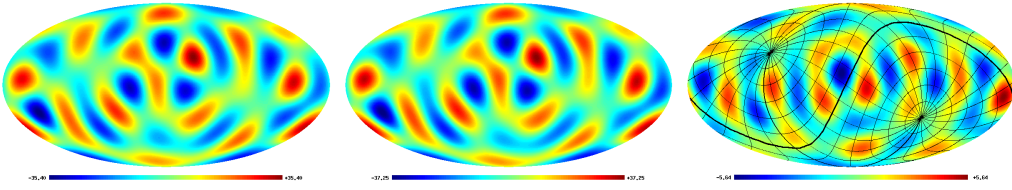


Figure 6: Left to right: the map of $\ell = 7$ of the Planck CMB map SMICA, the $\ell = 7$ of the ILC WMAP9 map, and the map of these signals difference. The ecliptic coordinate grid is overlaid on the map of difference.

position of spots along the Galactic plane, sensitivity of difference map at $\ell = 5$ to the equatorial coordinate system (equatorial poles are placed in singular points – saddles), and the axis of the multipole $\ell = 7$ lays on the Galactic plane and simultaneously, the saddle points of $\ell = 7$ are placed in ecliptic poles. The map of multipole difference at $\ell = 13$ (angular size of $\sim 6.5^\circ$) contains a feature similar to the harmonic $\ell = 7$ where the ecliptic poles are placed in singular points – local map minima and maxima. The multipole difference at the scales $\ell = 29$ ($\sim 3^\circ$) and $\ell = 37$ ($\sim 2.5^\circ$) contains a similar structure of spots placement. One line drawn by the very contrast spots formed with m -modes combinations of the $\ell = 29$ and $\ell = 37$ coincides with the ecliptic plane. Curiously, that a structure of the bright spots placement for $\ell = 29$ and $\ell = 37$ in the right hemisphere corresponds the anisotropic model Bianchi_{VIII} discussed in [10]. There is the range of multipoles ($\ell \in [41; 46]$) where the spectrum strongly differ for the WMAP and Planck data (Figs. 4, 7). The map difference for these multipole range shows the extended structure near the Galactic center.

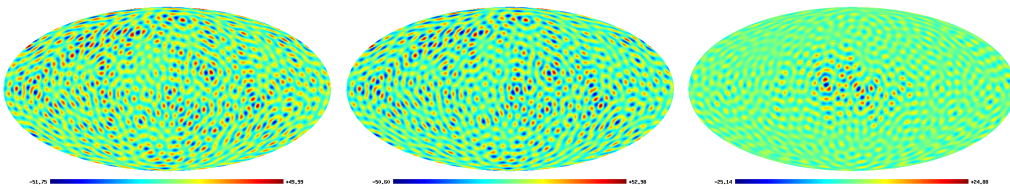


Figure 7: Left to right: the summarized signal of multipole $\ell \in [41, 46]$ for the Planck CMB map SMICA, harmonics $\ell = 41-46$ of WMAP9 ILC, and difference of these signals.

Note, that there are two important moments observed in multipole differences. First, all the maps of multipole difference with high amplitude contain features tied with galactic, ecliptic or/and equatorial (terrestrial) coordinate systems. Second, there is the $\Delta\ell = 8$ period for multipoles numbers having a big difference in amplitude. Peculiar harmonics have numbers $\ell = 5, 13, 29, 37, 45$.

4 Summary

As we can see from the details of the CMB anomalies mentioned above, most of them manifest the properties sensitive to local environment. Three main environments of the cosmic observatory are displayed in the CMB signal distribution. They are our Galaxy, the Solar (ecliptic) system and some features from the equatorial system. The Galaxy is a source of the non-Gaussian residuals visible in CMB spots positions (see [21]). The Cold Spot is a feature visible on a synchrotron map and on a map of the Faraday rotation depth. It could be due to any ionized cloud from Galaxy or its vicinity.

The Solar system objects are an additional residual source on the CMB map which is difficult to account using standard component separation methods. Possible sources of a residual signal are the antenna far sidelobes sensitive to the Sun and bright planets, a solar wind focusing by the Earth magnetosphere and passing through the Lagrange point L2, the objects at boundary of Solar system like the Kuiper belt.

The equatorial system features detected in some CMB correlation maps or in the single harmonic maps can be due by the influence of the Earth microwave emission via the antenna back lobes or possible Solar wind emission modulated by the Earth magnetosphere where the magnetic axis is close the Earth rotation axis.

It is necessary to note that there are some anomalies in the Planck data detected at high ($\ell > 600$) harmonics. There is a disagreement between cosmological parameters determination using the CMB angular power spectrum (including or not other experiments) and using only the Sunyaev–Zeldovich clusters [27]. Such a discordance, as discussed also in this paper, can be explained by the biased estimates of cluster parameters with the X-ray data.

And we can note that

- 1) WMAP and Planck data have practically the same low multipole anomalies, all the visible anomalies probably can be understood in the frame of the local (galactic and ecliptic) sources of microwave emission,
- 2) the difference of WMAP and Planck power spectra looks like one due to systematic effects of maps preparation (e.g. due to beam residuals).

Acknowledgments. Author is thankful to Conference Organizing Committee for hospitality. Author is also grateful to NASA for possibility to use NASA Legacy Archive where WMAP maps stored and ESA for open access to observational results in the Planck Legacy Archive. The GLESP (<http://www.glesp.nbi.dk>) package [28] was used to process the CMB maps on a sphere.

References

1. *C.L. Bennett, M. Halpern, G. Hinshaw et al.*, *Astrophys. J. Suppl.*, **148**, 1, 2003.
2. *N. Jarosik, C.L. Bennett, J. Dunkley et al.*, *Astrophys. J. Suppl.*, **192**, 14, 2011.
3. *C.L. Bennett, D. Larson, J.L. Weiland et al.*, *Astrophys. J. Suppl.*, **208**, 20, 2013.
4. *Planck Collaboration*, *Astron. Astrophys.* **571**, A1, 2014.
5. *C.L. Bennett, R.S. Hill, G. Hinshaw et al.*, *Astrophys. J. Suppl.*, **192**, 17, 2011.
6. *K. Land, J. Magueijo*, *Phys. Rev. Lett.*, **95**, 071301, 2004.
7. *M. Cruz, E. Martinez-Gonzalez, P. Vielva, L. Cayon*, *Mon. Not. Roy. Astron. Soc.*, **356**, 29, 2005.
8. *J. Kim, P. Naselsky*, *Astrophys. J. Lett.*, **714**, L265, 2010.
9. *H.K. Eriksen, F.K. Hansen, A.J. Banday et al.*, *Astrophys. J.*, **605** 14, 2014.
10. *Planck Collaboration*, *Astron. Astrophys.*, **571**, A23, 2014.
11. *S.M. Leach, J.-F. Cardoso, C. Baccigalupi et al.*, *Astron. Astrophys.*, **491**, 597, 2008.
12. *C.J. Copi, D. Huterer, D.J. Schwarz, G.D. Starkman*, *Mon. Not. Roy. Astron. Soc.*, **367**, 79 (2006).
13. *A. Gruppuso, C. Burigana, J. Cosmol. Astropart. Phys.*, **08**, 004, 2009.
14. *M. Demianski, A.G. Doroshkevich*, *Phys. Rev. D*, **751**, 3517, 2007.
15. *T. Koivisto, D.F. Mota, J. Cosmol. Astropart. Phys.*, **06**, 018, 2008.
16. *P.D. Naselsky, O.V. Verkhodanov*, *Astrophys. Bull.*, **62**, 203, 2007.
17. *P.D. Naselsky, O.V. Verkhodanov, M.T.B. Nielsen*, *Astrophys. Bull.*, **63**, 216, 2008.
18. *A.G. Doroshkevich, O.V. Verkhodanov*, *Phys. Rev. D*, **83**, 3002, 2011.
19. *C.J. Copi, D. Huterer, D.J. Schwarz, G.D. Starkman*, *Mon. Not. Roy. Astron. Soc.*, **449**, 3458, 2015.
20. *L. Rudnick, S. Brown, L.R. Williams*, *Astrophys. J.*, **671**, 40, 2007.
21. *O.V. Verkhodanov*, *Phys. Usp.*, **55**, 1098, 2012.
22. *P.D. Naselsky, P.R. Christensen, P. Coles et al.*, *Astrophys. Bull.*, **65**, 101, 2010.
23. *M. Hansen, W. Zhao, A.M. Frejsel et al.*, *Mon. Not. Roy. Astron. Soc.*, **426**, 57, 2012.
24. *F.K. Hansen, A.J. Banday, K.M. Górski*, *Mon. Not. Roy. Astron. Soc.*, **354**, 641, 2004.
25. *C.-G. Park*, *Mon. Not. Roy. Astron. Soc.*, **349**, 313, 2004.
26. *O.V. Verkhodanov*, *Astrophys. Bull.*, **69**, 330, 2014.
27. *Planck Collaboration*, *Astron. Astrophys.*, **571**, A20, 2014.
28. *A.G. Doroshkevich, O.V. Verkhodanov, P.D. Naselsky et al.*, *Int. J. Mod. Phys. D*, **20**, 1053, 2011.

* The color figures are available online in the Proceedings at <http://www.astro.spbu.ru/sobolev100/>.